

Broad-Band Rapid Tuning of a Single-Frequency Diode-Pumped Neodymium Laser

James Harrison, Andrew Finch, John H. Flint, and Peter F. Moulton, *Senior Member, IEEE*

Abstract—Over 600 mW has been obtained from a single-frequency Nd:YAG ring laser pumped by two 1 W diode lasers. Tuning over 50 GHz in less than 5 ms was achieved with a galvanometer-controlled, intracavity etalon. Locking to an external reference cavity has also been demonstrated.

I. INTRODUCTION

THE high power-per-unit-volume and ability to store energy for Q -switched operation make neodymium (Nd)-doped solid-state lasers particularly attractive for LIDAR systems. The majority of Nd-laser LIDAR's have been used for range-finding applications, with single-pulse transmitters, direct-detection receivers, and simple time-of-flight signal processing. Coherent-detection LIDAR systems, for more sophisticated measurements, such as target velocity and vibration spectra, have typically employed CO₂ gas lasers, which historically have been more readily operated with stable, single-frequency output. Recently, with the widespread development of diode-laser pumping techniques, Nd-doped stable-single-frequency lasers have become available, and one can consider implementation of practical, Nd-laser-based coherent LIDAR systems.

At the heart of any coherent LIDAR system is the CW single-frequency master oscillator, which might be employed, for example, both as an injection-seeding source for a pulsed transmitter and as a local oscillator for the detection system. In some coherent LIDAR systems requiring detection of multiple targets with widely varying velocities, the frequency of the master oscillator must be adjustable to maintain the detected signal within the bandwidth of the receiver electronics. The work described in this paper is motivated by the need for a master oscillator that can be frequency-tuned in less than 20 ms to arbitrary points within at least a 30 GHz span. While the maximum allowable spectral width at any operating frequency depends on the exact LIDAR application, the width is likely to be in the range of 1–100 kHz. The goal of this work has been the demonstration of a CW diode-pumped Nd laser capable of meeting these requirements while operating at a power level of at least 100 mW.

Manuscript received July 19, 1991; revised September 18, 1991. This work was supported by the SBIR program of SDIO and administered by NOSC under Contract N66001-88-C-0095.

The authors are with the Research Division, Schwartz Electro-Optics Inc., Concord, MA 01745.

IEEE Log Number 9106644.

Broad-band rapid tuning of diode-pumped Nd lasers has been achieved with piezo-electric [1]–[3] and electrooptic control of the cavity length [4]. With these methods, the laser frequency may be scanned over a single longitudinal mode, and thus miniature resonators are required to obtain scan ranges in excess of 1 GHz. Monolithic structures [1], [2], [5], [6], in particular, can be may very short and offer superior frequency stability. Owyong and Esherrick [1] have demonstrated piezo-electric tuning over 76.5 GHz with 1.0 mm monolithic Nd:YAG standing-wave laser. However, single-frequency operation of such lasers is limited to low powers (~ 1 mW). Schultz and Henion [4] observed single-frequency operation at output powers up to 20 mW (with a Ti:Al₂O₃ pump laser) with a Nd:YAG standing-wave resonator consisting of discrete components, including an electrooptic modulator that provided a tuning range of 12.5 GHz. The problem of multimode operation was overcome with the development of monolithic ring lasers [5], although the tuning range of such devices is ultimately limited by the path length of the ring. Kane and Cheng [2] reported a scan range of only 100 MHz for their piezo-electrically tuned, monolithic, Nd:YAG ring laser, well below the longitudinal mode spacing of ~ 15 GHz. Trutna and Donald [3] achieved the maximum scan range of 13.5 GHz with a similar resonator that was composed of two sections separated by a variable air gap.

The approach taken here has been to employ a ring resonator [7], [8] including one or two discrete, longitudinally pumped, Nd-doped gain elements, with a longitudinal mode spacing of 0.46 GHz. Rapid tuning over the gain spectrum, covering many longitudinal modes, is achieved by controlling the incident angle of an intracavity etalon that is mounted on a galvanometer. Frequency control within a single longitudinal mode is obtained by fine translation of a resonator mirror. Experimental results include the generation of over 600 mW in a single-frequency diffraction-limited beam with a Nd:YAG laser pumped by a pair of 1 W diode lasers. Demonstrations of broad-band tuning include a frequency step of 50 GHz with a settling time of less than 5 ms.

The following sections provide details of the laser design and performance. These include both resonator (Section II), pumping-image (Section III), and tuning (Section IV) considerations. Data obtained here are shown to be in excellent agreement with two-dimensional models employed in the design. Rapid-tuning data presented in Sec-

tion V document the response of the laser frequency to a step change in etalon position. These were obtained by monitoring the output of an interferometer that was tuned to the target frequency. Also included in that section are heterodyne data that were derived from two similar lasers, with the lasers either free-running or locked to an external reference cavity. The full width at half maximum (FWHM) of the heterodyne signal obtained with two lasers independently stabilized to the reference cavity was 50 kHz in a 50 s scan.

II. RESONATOR DESIGN

Fig. 1 is schematic of the Nd ring laser employed here. The resonator consists of a Nd active mirror, a flat high-reflectivity (HR) mirror, and two curved (50 cm radius of curvature) mirrors (one coated for HR and one a partially transmitting output coupler). The interior surface of the Nd slab is antireflection (AR) coated for 1064 nm while the external surface has a dichroic coating for HR at 1064 nm and high transmission in the pump region around 800 nm. The four mirrors are arranged in a figure-eight pattern with the curved HR mirror mounted to a piezo-electric translator (PZT) to allow continuous tuning within the oscillating longitudinal mode determined by the intracavity etalon. Unidirectional operation is enforced by an intracavity optical diode [9] that consists of a terbium gallium garnet Faraday element and an optically active quartz plate, each designed for 2° polarization rotation at the laser wavelength. Pump light is provided by a single 1 W diode laser (Spectra Diode Laboratories SDL-2462-P1) that is imaged in the active mirror by the beam-conditioning optics.

Two beam waists occur within the resonator: one centered between the active mirror and the HR flat mirror and one centered between the two curved mirrors. The radius of the TEM₀₀ mode throughout the resonator is displayed in Fig. 2. The mode is traced as a function of position beginning and ending at the 50 cm, HR mirror ("0 cm", and "65.2 cm"). The calculated longitudinal-mode spacing of the resonator is $\Delta f_L = 453$ MHz.

Laser performance can be analyzed using a two-dimensional model for a longitudinally pumped system in which both lasers are assumed to operate in a fundamental Gaussian mode [10]. The CW threshold power P_{TH} for a ring resonator, measured at the output of the pump laser, is given by the following expression:

$$P_{TH} = \eta_c \frac{\pi h \nu_p}{2\sigma\tau} (T + L_{CAV} + L_{XTL}) \cdot (w_o^2 + w_p^2)(1 - \exp[-\alpha l])^{-1} \quad (1)$$

where η_c is the coupling efficiency between the pump laser and the gain element, $h\nu_p$ is the pump photon energy, σ is the emission cross section, τ is the upper-state lifetime, and the final term in brackets represents the pump-absorption efficiency (α is the absorption coefficient at ν_p and l is the length of gain element). The $1/e^2$ -intensity radii of the resonator mode and pump beam in the active region

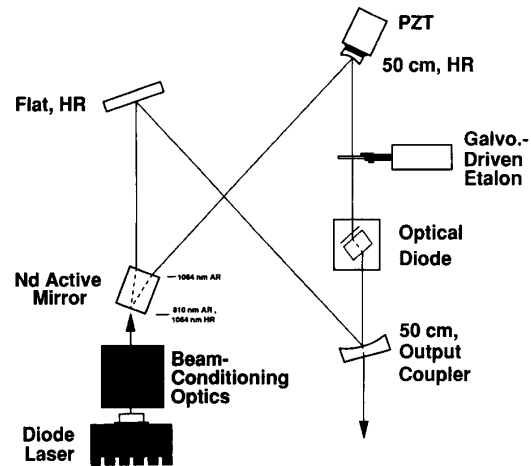


Fig. 1. Schematic of the laser resonator.

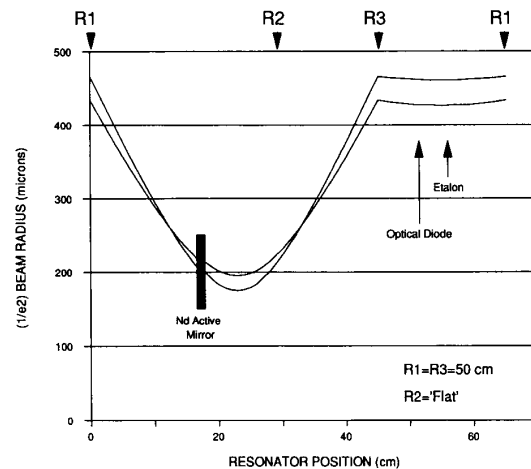


Fig. 2. Tangential and sagittal TEM₀₀ mode radii as a function of position in the resonator.

are given by w_o and w_p , respectively. The round-trip resonator losses consist of T (transmission losses), L_{CAV} (intracavity losses exclusive of the gain element), and L_{XTL} (losses in the gain element, e.g., scattering and parasitic absorption).

The relation for the laser slope efficiency η_s is

$$\eta_s = f_{ovl} \eta_c (\nu_o / \nu_p) \left(\frac{T}{T + L_{CAV} + L_{XTL}} \right) (1 - \exp[-\alpha l]) \quad (2)$$

where f_{ovl} is an overlap parameter representing the fraction of the absorbed pump power that falls within the volume of the TEM₀₀ mode in the active mirror, and the first bracketed term is the quantum defect.

A general characteristic of the laser designs studied here is that the cross section of the TEM₀₀ mode is approximately constant, and slightly elliptical, throughout the active mirror. Therefore, equating w_o in (1) to the average

of the tangential and sagittal radii is a straightforward approximation. Things are more complicated when w_p is considered. In applying the model to the diode-pumped Nd ring lasers, a basic assumption has been violated since the diode lasers employed here are not generally diffraction-limited sources. However, by determining the pump distribution in the active mirror, it is possible to make reasonable estimates for w_p and f_{ovl} . For efficient operation, the pump-imaging system is designed so that the pump beam underfills the TEM₀₀ mode volume in the active region. In this case, w_p is approximately equal to the average radius of the pump beam in the absorption region and $f_{ovl} = 1$.

Note that a two-dimensional model has been applied to solve what is in fact a three-dimensional problem. To determine a more accurate effective radius w_p , the radius of the pump beam should be averaged over the entire cross section (i.e., over 2π radians) throughout the active region with proper weighting to account for the exponential absorption of power [11]. In practice, estimates for w_p have been based on modeling and measurement of the pump-beam distribution. The resulting uncertainty is low enough that we find good agreement between calculations based on the model and experimental results.

Calculated laser performance based on (1), and (2) is summarized in Table I. The two columns list results of calculations for two similar lasers including either $l = 0.6$ cm or $l = 0.8$ cm Nd:YAG active mirrors. Input parameters were chosen to match the two lasers that are characterized in Section V. Other parameters used in the calculations are $\sigma = 3.3 \times 10^{-19}$ cm² [12], $\tau = 255$ μ s [12], $T = \{2.7\%, 2.3\%\}$, $L_{CAV} = 1.7\%$ (derived from measurements of the power dependence of the relaxation-oscillation frequency), $L_{XTL} = 0$, $w_o = 212.5$ μ m, $w_p = 200$ μ m, $\alpha = 4.1$ cm⁻¹, $\eta_c = 0.95$ (corresponding to the transmission of the active mirror at the pump wavelength), and $f_{ovl} = 1$. The results indicate $P_{TH} < 200$ mW (incident on the active mirror) and $\eta_s = 40\%$. Note that the absorption coefficient used here was experimentally determined; it represents an average over the spectrum of the diode laser with the device temperature-tuned for maximum absorption. The corresponding absorption efficiencies are 91% for a 6 mm crystal and 96% for an 8 mm crystal.

III. PUMP IMAGING

The pump optics consist of a collimating lens, two intermediate cylindrical telescopes (with orthogonal orientation) and a focussing lens. A schematic is provided in Fig. 3. Individual lenses were AR-coated for use in the pump region around 800 nm. A key aspect of the design is that the two orthogonal telescopes have mutually inverse magnifications ($M_{TEL} = 6.3x$ in the plane of the laser-diode junction, $M_{TEL} = 0.16x$ in the plane perpendicular to the junction). This facilitates packaging by allowing similar lens pairs to be fixed back-to-back in such a way that both telescopes are aligned at once by adjusting

the spacing between the lens pairs. In either plane, the overall magnification m is given by

$$m = f_{FOC}/(f_{COLL}M_{TEL}) \quad (3)$$

where $f_{COLL} = 8.18$ mm and $f_{FOC} = 50.0$ mm are the focal lengths of the collimating and focusing lenses. In order to achieve a good spatial match over the absorption region, one-to-one imaging (i.e., $m = 1$) is employed in the parallel plane.

A geometric model has been used to facilitate the design of the beam-conditioning optics by determining the envelope of the pump-radiation in the active mirror. Given the dimensions of the diode-laser emission region and the divergence angles, ray-tracing through the sequence of lenses provides a description of the image in the active mirror. Use of this model is based on the assumption that efficient pumping requires the pump light to underfill the mode volume in the absorption region, independent of the details of the spatial distribution of the beam. The model is only used to determine a solid conical volume that contains all but a negligible portion of the pump radiation in the gain element. Note that while this is a valid assumption for the 1064 nm transition in Nd, it is not generally applicable to quasi-three-level laser systems (e.g., the 946 nm Nd line) [13].

Two similar pump modules (referred to here as PM-1 and PM-2) were aligned and tested. In both cases the overall transmission measured from the diode laser to the output of the focusing lens (which was primarily determined by reflection losses) was $>90\%$. The output-beam profiles of both modules were measured in the focal region with a commercial diagnostic system (Big Sky Software MULTICAM), with resolutions of 27 μ m in the plane of the diode-laser junction and 23 μ m in the plane perpendicular to the junction. Data were obtained with translation of the camera along the beam axis. For comparison with these data, the geometric model was used to calculate the image in air. Fig. 4 shows the image dimensions in a region ± 5 mm from the focal plane along with the results of beam-profile measurements obtained with both pump modules. The data points correspond to the beamwidths within which $>90\%$ of power was contained.

IV. TUNING

The PZT-controlled resonator mirror provides a mechanism for fine tuning the laser over a range of approximately $\pm \Delta f_L/2 = \pm 227$ MHz, as determined by the longitudinal mode spacing Δf_L . Tuning the laser over a much wider range, covering much of the gain spectrum of the active medium, was achieved by controlling the intracavity etalon. In this case, the laser frequency was scanned through adjacent longitudinal modes of the resonator. Here the required range, 30 GHz, corresponds to a maximum scan of ~ 66 modes. Note that this is well within the ~ 180 GHz gain bandwidth of the 1064 nm transition in Nd:YAG.

TABLE I
LASER-PERFORMANCE CALCULATIONS

Input Parameters:		
η_c	95%	95%
pump wavelength	808 nm	808 nm
laser wavelength	1064 nm	1064 nm
σ	$3.3 \times 10^{-19} \text{ cm}^2$	$3.3 \times 10^{-19} \text{ cm}^2$
τ	255 μs	255 μs
L_{CAV}	1.7%	1.7%
L_{XTL}	0%	0%
T	2.7%	2.3%
$2w_o$	425 μm	425 μm
$2w_p$	400 μm	400 μm
α	4.1 cm^{-1}	4.1 cm^{-1}
f_{opt}	1.0	1.0
l	6.0 mm	8.0 mm
Calculated results:		
P_{TH}	198 mW	171 mW
η_s	40%	40%

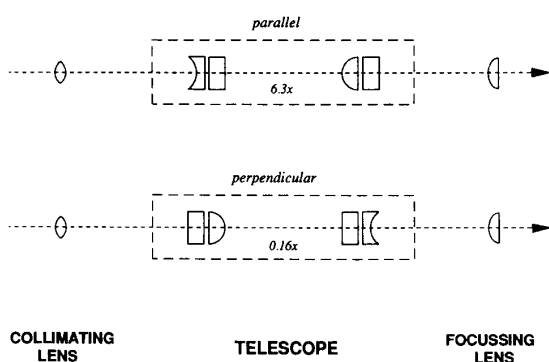


Fig. 3. Schematic of the imaging system: view parallel to the plane of the diode-laser junction (upper), and view perpendicular to the junction plane (lower).

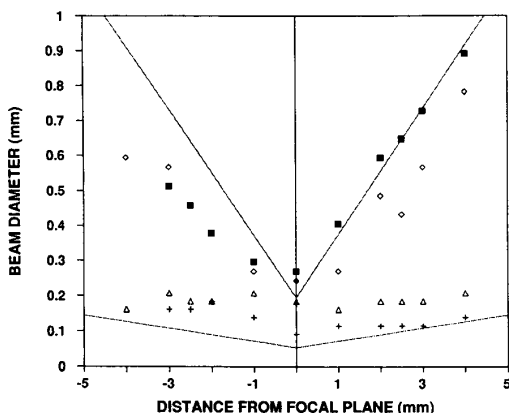


Fig. 4. Measured image dimensions in the focal region: PM-1 (parallel plane—"diamond," perpendicular plane—"triangle"), PM-2 (parallel plane—"square," perpendicular plane—"plus"). Calculated dimensions for images in air are also shown ("solid lines").

The galvanometer-controlled solid etalon proved to be a simple and reliable means of achieving the desired tuning. To find an expression for the dependence of the laser

frequency on the etalon angle, we begin with the resonance condition for the etalon:

$$M\lambda_R = 2nt \cos \left(\sin^{-1} \left[\frac{\sin \theta}{n} \right] \right) \quad (4)$$

where M is an integer, λ_R is the resonant wavelength, n is the refractive index of the etalon, t is the etalon thickness, and θ is the angle of incidence. Near normal incidence (i.e., $\theta \sim 0$), the angular dependence can be simplified after a series expansion. This yields the approximate relation for the resonant frequency ν_R [14]

$$\nu_R = \frac{Mc}{2nt} \left(1 + \frac{\theta^2}{2n^2} \right) \quad (5)$$

where c is the vacuum speed of light. Taking the derivative with respect to angle, the rate of change in the etalon resonance with angle (i.e., the tilt-tuning rate) is given by

$$\frac{\delta \nu_R}{\delta \theta} = \frac{\nu_R \theta}{n^2}. \quad (6)$$

It is evident from (6) that the tuning rate increases linearly with angle. As the etalon is rotated away from normal incidence, the laser frequency increases in steps equal to Δf_L until an etalon mode hop occurs. At the etalon mode hop, the laser frequency jumps back by an amount equal to the free spectral range (FSR) of the etalon. As the tilt angle is increased further, the frequency will scan again over the same range until another etalon mode hop occurs. The FSR of the 1.0 mm etalons used here is 103 GHz.

V. LASER PERFORMANCE

Input/Output Characterization

Output power versus absorbed pump power is plotted for the two single-frequency Nd:YAG lasers in Fig. 5, where the absorbed power includes the light reflected at the input facet of the active mirror in addition to that actually absorbed. The data, which are in close agreement with the calculations of Table I, were obtained at 1064 nm

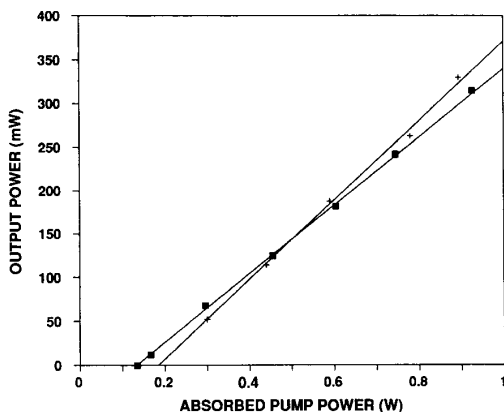


Fig. 5. Output power versus absorbed pump power ($l = 8$ mm, $T = 2.3\%$ - "square," $l = 6$ mm, $T = 2.7\%$ - "plus").

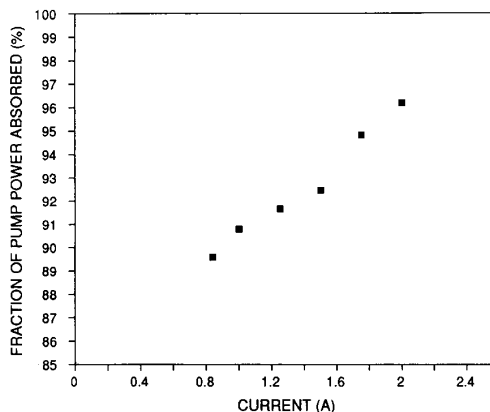


Fig. 6. Percentage of the incident pump power absorbed in the 8 mm, Nd:YAG active mirror versus diode-laser current.

without the intracavity etalon. The temperature of the diode-laser submount was maintained at 9.0°C during the measurements so that the absorption efficiency varied with the operating point. Fig. 6 shows the experimental absorbed fraction as a function of current with the 8 mm active mirror and the diode-laser submount at 9.0°C . In principle, maximum absorption could be maintained over a wide current range by changing the diode-laser temperature.

The addition of a 1 mm thick, uncoated, fused-silica etalon resulted in a small reduction in efficiency. This is evident in the data of Fig. 7 which were obtained with the 8 mm active mirror. It is interesting to note that in contrast to this, when the laser was operated at 1047 nm with a Nd:YLF active mirror no reduction in power was observed with the insertion of the etalon.

In principle, additional diode lasers can be added to the system to substantially increase the power of the Nd laser. Up to four diode lasers could be included in a simple configuration by summing orthogonally polarized lasers in pairs with two polarizing beam splitters placed after the collimating lenses. Each pair of lasers could then be imaged through a common focusing lens to pump both legs of the beam path in the active mirror. Additional scaling can be achieved by replacing the flat, HR mirror with a second active mirror. Data obtained with two Nd:YAG active mirrors (6 mm, 8 mm), each pumped by a single diode laser, with the intracavity etalon and $T = 2.7\%$, are shown in Fig. 8.

Tuning Experiments

By employing the full range of the galvanometer (General Scanning G120-DT), it was possible to tune the etalon through more than seven orders on either side of normal incidence (i.e., zeroth order). Fig. 9 is a map of the experimental transition points between all accessible orders, indicating the characteristic parabolic dependence [(5)] over the entire galvanometer range. Having established that the etalon tuning characteristics were in good

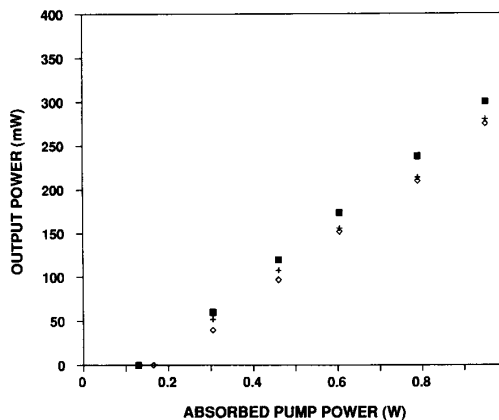


Fig. 7. Output power versus absorbed pump power ($T = 2.3\%$, without etalon - "square," $T = 2.3\%$, with etalon - "plus," $T = 2.7\%$, with etalon - "diamond").

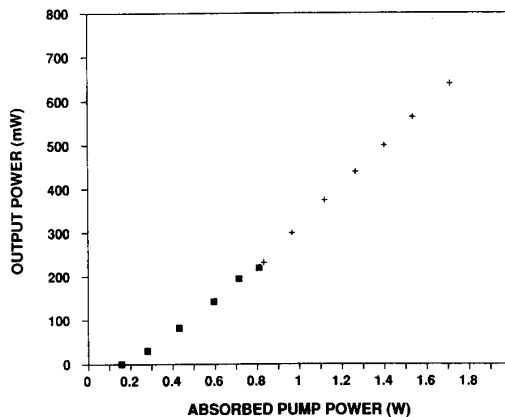


Fig. 8. Output power versus absorbed pump power with an intracavity etalon and two active mirrors (PM-1 off and PM-2 on - "square," PM-1 and PM-2 on - "plus").

agreement with theory, a series of measurements were conducted to document the step response of broad-band, rapid tuning. The basic experiment consisted of driving

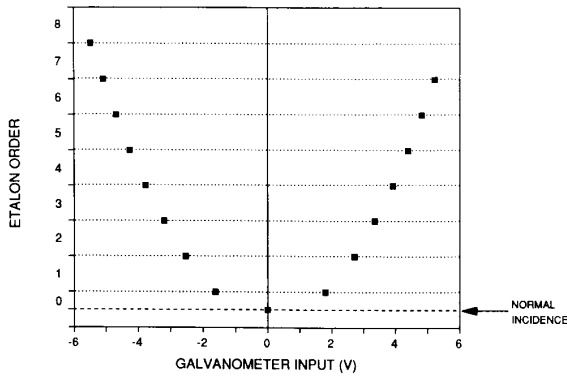


Fig. 9. Transition points between etalon orders.

the galvanometer with a square wave to shift the laser between two frequencies with a predetermined separation. The transition between frequencies was observed by recording the transmission of a 2 GHz FSR Fabry-Perot interferometer. This instrument was particularly useful because the peak-to-peak frequency fluctuations following a step transition typically fell between the 10 and 90% transmission points on one side of the transmission peak. In addition, it was sufficiently stable that the observed frequency fluctuations were characteristic of the laser alone. Over the course of the experiment, the temporal response of the laser frequency to steps in the range of 0.46 GHz (i.e., between adjacent longitudinal modes) to 50 GHz were recorded with a transient digitizer. Frequency steps in excess of 2 GHz were calibrated with a 150 GHz FSR scanning interferometer.

The response of the 2 GHz FSR interferometer was calibrated in terms of the transmission versus frequency deviation by observing the transmission in scanning mode. Step-response data were obtained with the interferometer bias adjusted so that the target frequency corresponded to the half-power point on (for example) the high-frequency side of the fringe peak.

In the current system, the laser-frequency step response is determined primarily by the response of the galvanometer. The latter resembles a well-behaved, damped, second-order system. The trade-off between rise time and overshoot can be adjusted electronically. Step-tuning experiments presented here were conducted with the galvanometer either over-damped or under-damped. The corresponding normalized step-responses are shown in Fig. 10.

Data for an overdamped, 5 GHz step are displayed in Fig. 11. These were obtained with the laser operating at 150 mW near the gain peak in first order prior to the step at time zero. Note that the linear transmission scale corresponds to a nonlinear frequency scale where transmissions of 0.6 and 0.4 indicate frequency fluctuations of 4.6 and -5.6 MHz, respectively, relative to the half-power point. The two sets of data were obtained with adjustment of the PZT voltage to indicate the range over which the turn-on delay could be varied. This phenomenon derives

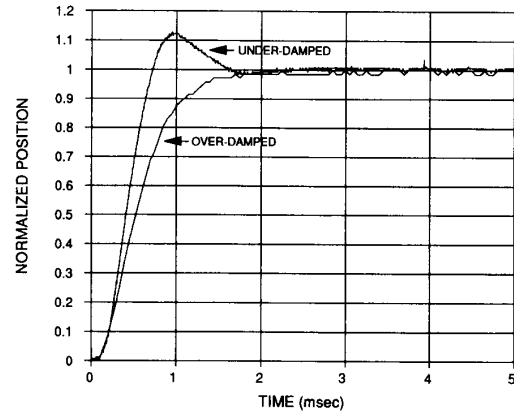


Fig. 10. Experimental settings of the galvanometer step response.

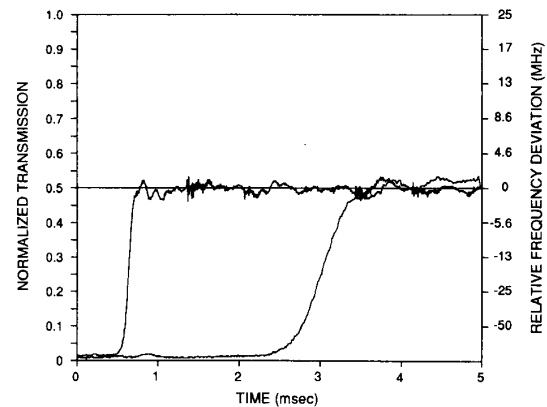


Fig. 11. Laser-frequency step response at two positions of the PZT (150 mW, 5 GHz step, over-damped).

from the fact that varying the position of the PZT alters the offset at the target frequency between the resonator mode and the etalon peak. The highest sensitivity occurs with relatively small steps where the transition between adjacent longitudinal modes is a significant portion of the total tuning range.

Typical data obtained at 150 mW with the galvanometer under-damped, for steps in first order of 0.46, 5, 25, and 50 GHz are displayed in Fig. 12. Peaks evident before the turn-on of the target longitudinal mode are signatures of intermediate modes that overlapped with a transmission window as the galvanometer was slewing between end points. The under-damped data are characterized by shorter turn-on delays and higher peak-to-peak fluctuations during the subsequent settling period than the corresponding over-damped data. Fig. 13 provides a direct comparison of typical 25 GHz step data for both settings of the galvanometer. The same data are again plotted together in Fig. 14, which also includes over-damped data obtained with a 25 GHz step in the fourth order of the etalon. Note that the peak-to-peak fluctuations in the fourth order, where the tuning rate is considerably higher,

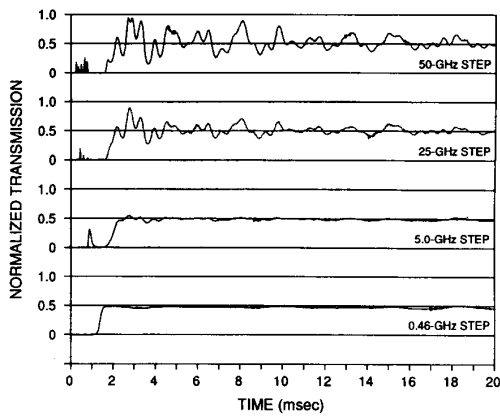


Fig. 12. Laser-frequency step response for step sizes of 0.46, 5, 25, and 50 GHz (150 mW, under-damped).

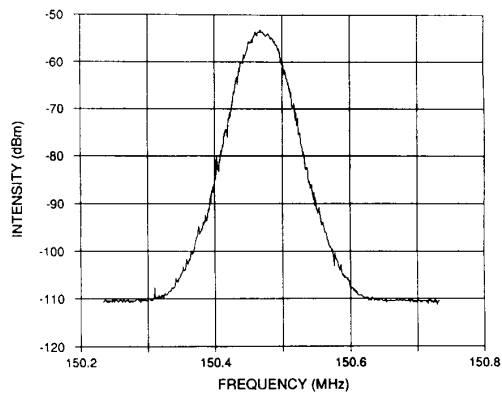


Fig. 15. Heterodyne data obtained with both lasers locked to the reference interferometer (10 kHz/s scan rate).

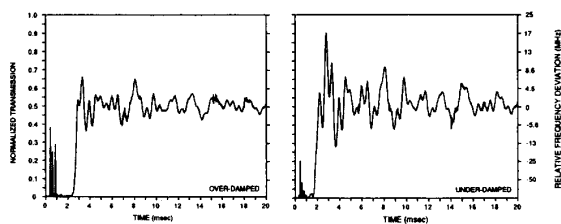


Fig. 13. Laser-frequency step response: over-damped and under-damped (150 mW, 25 GHz step).

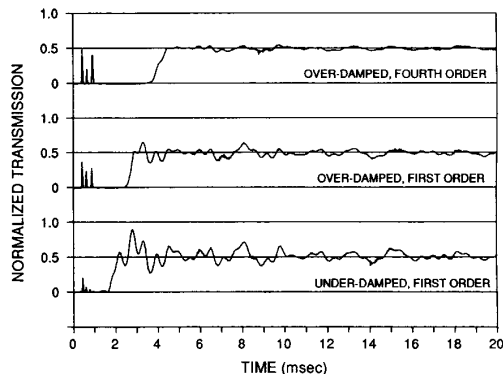


Fig. 14. Laser-frequency step response (150 mW, 25 GHz step): first order (over-damped and under-damped) and fourth order (over-damped).

are significantly smaller than those of the corresponding first-order data. This supports the general conclusion that these fluctuations are related to the electromechanical response of the galvanometer. They increase with the angular motion of the galvanometer and are not indicative of fundamental laser dynamics.

While all of the step-tuning data presented here was obtained at the 150 mW operating point, experiments were conducted at a wide range of powers with similar results. Fluctuations in the laser intensity, which were dominated by current-driven pump-power fluctuations, were also

monitored during the experiments. While the output power was dependent on the operating point and the etalon position, the relative intensity fluctuations appeared to be independent of the laser frequency. The step change in power generally increased with step size and the proximity of the operating point to threshold. For example, with a 50 GHz step, the change in power was 62% at a nominal operating point of 25 mW while only a 6% change was observed at 150 mW. With steps of 5 and 0.46 GHz, the changes in power were 4% and less than 1%, respectively, at both operating points.

Heterodyne measurements were used to characterize laser frequency noise and to demonstrate the stabilization required for the envisioned LIDAR system. A third interferometer (FSR = 150 MHz) was employed as a reference cavity/optical discriminator for frequency locking [15]. Control-loop error signals were derived from the interferometer transmission for feedback to the PZT's. After rotating the polarization of one beam, the two lasers were input to the interferometer with orthogonal polarizations and separated at the output with a polarization beam splitter. This allowed both lasers to be independently locked simultaneously to different orders of the interferometer. Typical heterodyne data obtained over 50 s with both lasers locked and operating at 150 mW are included in Fig. 15. The FWHM of the signal, representing the combined jitter of the two lasers, is < 60 kHz. The stability was limited here by noise in the high-voltage amplifiers employed in the control loops to drive the PZT's.

VI. SUMMARY

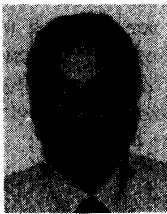
In conclusion, we have demonstrated rapidly tunable single-frequency diode-pumped Nd:YAG lasers. An output of 640 mW at 1064 nm was obtained with a pump power of 1.94 W (1.71 W absorbed) derived from two pump lasers. The laser has the potential for scaling to the 1-10 W range with additional diode lasers arranged for longitudinal pumping.

Broad-band rapid tuning with an intracavity etalon has been characterized. The laser-frequency step response is

dominated by the dynamics of the galvanometer. Turn-on times were typically within a factor of two of the 1.5–2 ms galvanometer settling time. A trade-off is possible between the turn-on delay and the settling time, depending on system requirements, by adjusting the galvanometer step response. The settling time appears to increase with the range of motion of the galvanometer. In addition, the turn-on delay is especially sensitive to the PZT position for relatively small steps.

REFERENCES

- [1] A. Owyong and P. Escherick, "Stress-induced tuning of a diode-laser-excited monolithic Nd:YAG laser," *Opt. Lett.*, vol. 12, pp. 999–1001, 1987.
- [2] T. J. Kane and E. A. P. Cheng, "Fast frequency tuning and phase locking of diode-pumped Nd:YAG ring lasers," *Opt. Lett.*, vol. 13, pp. 970–972, 1988.
- [3] W. R. Trutna, Jr. and D. K. Donald, "Two-piece, piezo-electrically tuned, single-mode Nd:YAG ring laser," *Opt. Lett.*, vol. 15, pp. 369–371, 1990.
- [4] P. A. Shultz and S. R. Henion, "Frequency-modulated Nd:YAG laser," *Opt. Lett.*, vol. 16, pp. 578–580, 1990.
- [5] T. J. Kane and R. L. Byer, "Monolithic, unidirectional single-mode Nd:YAG ring laser," *Opt. Lett.*, vol. 10, pp. 65–67, 1985.
- [6] J. J. Zayhowski and A. Mooradian, "Single-frequency microchip lasers," *Opt. Lett.*, vol. 14, pp. 24–26, 1989.
- [7] A. R. Clobes and M. J. Brienza, "Single-frequency traveling-wave Nd:YAG lasers," *Appl. Phys. Lett.*, vol. 21, pp. 265–267, 1972.
- [8] J. Harrison, G. A. Rines, P. F. Moulton, and J. R. Leger, "Coherent summation of injection-locked, diode-pumped Nd:YAG ring lasers," *Opt. Lett.*, vol. 13, pp. 111–113, 1988.
- [9] T. F. Johnston, Jr. and W. Proffitt, "Design and performance of a broad-band optical diode to enforce one-direction traveling-wave operation of a ring laser," *IEEE J. Quantum Electron.*, vol. QE-16, pp. 483–488, 1980.
- [10] P. F. Moulton, "An investigation of the Co:MgF₂ laser system," *IEEE J. Quantum Electron.*, vol. QE-21, pp. 1582–1595, 1985.
- [11] A. J. Alfrey, "Modeling of longitudinally pumped CW Ti:Al₂O₃ laser oscillators," *IEEE J. Quantum Electron.*, vol. 25, pp. 760–766, 1989.
- [12] A. A. Kaminskii, *Laser Crystals*. New York: Springer-Verlag, 1990, p. 240.
- [13] W. P. Risk, "Modeling of longitudinally pumped solid-state lasers exhibiting reabsorption losses," *J. Opt. Soc. Amer. B*, vol. 5, pp. 1412–1423, 1988.
- [14] G. K. Klauminzer, "Etalon/grating synchronized scanning of a narrowband pulse dye laser," *Opt. Eng.*, vol. 13, pp. 528–530, 1974.
- [15] R. L. Barger, M. S. Sorem, and J. L. Hall, "Frequency stabilization of a cw dye laser," *Appl. Phys. Lett.*, vol. 22, pp. 573–575, 1973.



James Harrison was born in New Haven, CT, on May 31, 1956. He received the B.S., M.S., E.E., and Ph.D. degrees from the Department of Electrical Engineering and Computer Science, Massachusetts Institute of Technology, Cambridge, where he was awarded the N.C.R. Fellowship for 1985–1986. His doctoral dissertation, completed in 1986, involved a study of the spectral properties of semiconductor diode lasers and included the development of ultrastable external cavity lasers. This work was performed in the Quantum

Electronics Group at M.I.T. Lincoln Laboratory, Lexington.

From 1981 to 1982 he was an Electronics Engineer in the Laser Isotope Separation Program at Lawrence Livermore National Laboratory, Livermore, CA. There he worked on the development of the dye master oscillator and performed a spectroscopic study of the source metal vapor. In 1985 he was a summer staff member at M.I.T. Lincoln Labs. Since 1987 he has been at Schwartz Electro-Optics, Research Division, Concord, MA. His work focuses on the development of single-frequency solid-state lasers. These include both pulsed and CW diode-pumped systems, and involve a variety of materials for visible, near-infrared, and eye-safe applications.

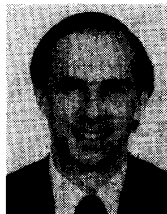
Dr. Harrison is a member of the Optical Society of America and Sigma Xi.



Andrew Finch was born in Birmingham, England in 1962. He received the B.A. degree in physics from Oxford University in 1984, and the M.Sc. degree in optoelectronics and laser devices, and the Ph.D. degree in laser physics from the University of St. Andrews, Scotland, in 1985 and 1989, respectively. His Ph.D. research included the study of mode-locked dye lasers and linear and nonlinear optical pulse diagnostics.

In 1987, he was employed as a research assistant at the University of St. Andrews developing optoelectronic time and frequency domain techniques to characterize high speed photodetectors. Since January 1990 he has been with the research division of Schwartz Electro-Optics, Concord, MA, where he is currently working on the development of diode-pumped frequency-stabilized Nd:YAG ring lasers.

John H. Flint, photograph and biography not available at the time of publication.



Peter F. Moulton (M'69-S'74-SM'84) was born in Springfield, MA, on May 27, 1946. He received the A.B. degree in physics from Harvard University, Cambridge, MA, in 1968 and the M.S. and Ph.D. degrees from the Department of Electrical Engineering and Computer Science, Massachusetts Institute of Technology, Cambridge, in 1971 and 1975, respectively.

He spent a post-Doctorate year in 1975 at M.I.T. Lincoln Laboratory, Lexington, and became a staff member there in 1976. His work at Lincoln Laboratory included high-resolution infrared spectroscopic measurements of molecules, development of lasers or remote sensing, and research and development of tunable and high-efficiency solid-state lasers. Since 1985 he has been Vice President and General Manager of the Research Division of Schwartz Electro-Optics, Concord, MA, where he is engaged in the research and development of a new solid-state laser materials and systems.

Dr. Moulton is a member of the Optical Society of America and Sigma Xi.